

Contents lists available at ScienceDirect

Chemical Physics

journal homepage: www.elsevier.com/locate/chemphys



Intersystem crossing dynamics in singly substituted thiouracil studied by time-resolved photoelectron spectroscopy: Micro-environmental effects due to sulfur position



Abed Mohamadzade^a, Shuming Bai^b, Mario Barbatti^{b,*}, Susanne Ullrich^{a,*}

- ^a Department of Physics and Astronomy, University of Georgia, Athens, GA 30602, USA
- ^b Aix Marseille Univ, CNRS, ICR, Marseille, France

ARTICLE INFO

Keywords:
Modified DNA bases
4-Thiouracil
Excited state dynamics
Internal conversion
Intersystem crossing
Photodynamics
Time-resolved spectroscopy
Pump-probe
Ultrafast spectroscopy

ABSTRACT

The ultraviolet (UV) photophysics of the natural and modified nucleobases can be surprisingly different. In response to UV radiation, the natural pyrimidine nucleobases undergo ultrafast internal conversion back to the ground state, whereas their thiobase analogues, in which an oxygen has been replaced by sulfur, instead display efficient intersystem crossing to the triplet manifold. Here, the effect of the substituent position is investigated with time-resolved photoelectron spectroscopy on 4-thiouracil, which is contrasted to previous work on 2-thiouracil. Although the photophysical pathway of both structural isomers is similar, i.e., leading from the S_2 ($^1\pi\pi^*$) state, via S_1 ($^1n\pi^*$), to the triplet manifold and subsequently back to the ground state, the intersystem crossing dynamics are strongly influenced by the surrounding intramolecular environment of the sulfur atom.

1. Introduction

The photophysics of modified nucleobases are particularly intriguing since small structural changes to the natural nucleobases, such as single atom substitutions, can have profound effects on their excitedstate deactivation pathways. The photodynamics of the natural bases predominantly proceed via ultrafast internal conversion along singletstate pathways, providing photostability and inherent protection against harmful UV radiation - crucial, for example, for survival under harsh environmental conditions as found on the early Earth [1-8]. In modified nucleobases, such as the pyrimidine thiobases, where one exocyclic oxygen has been replaced by sulfur, intersystem crossing populates the triplet manifold with high quantum yields [9-13]. Although trapping in the lowest triplet state reduces photoprotective properties, it also leads to long-lived, reactive states, which are highly desirable for pharmacological applications; for example, as photosensitizers for cancer treatment [13-18]. Besides, the diverse photoproperties of the thiobases are of fundamental photochemical interest. Intricate details of potential energy surfaces are modulated by subtle structural changes, causing drastic effects on the photodynamic response of the thiobases [3,9,13,19-22].

Such complex behavior is highlighted in the present gas-phase time-

resolved photoelectron spectroscopy (TR-PES) study, which investigates the effect of substituent position through comparison of the structural isomers 4-thiouracil (4-TU) and 2-thiouracil (2-TU) free from influences of a solvent. As will be discussed below, substitution of the oxygen in the 4- or 2-position, placing the sulfur atom into a slightly different intramolecular micro-environment, leads to significant changes in the dynamics.

While the solution-phase photophysics of the thiobases have been investigated extensively [9,19], gas-phase spectroscopic studies are currently sparse [3,10] and a summary of the relevant experimental and theoretical literature, with focus on thiouracils, is given below.

Concerning intersystem crossing in thiobases, low-lying singlet states of $^1n\pi^*$ character are emerging as a critical doorway for accessing the triplet manifold, and the intersystem crossing dynamics are governed by spin–orbit coupling constants and barrier heights to access crossing points [9,11,23]. This was verified in a recent TR-PES study of natural and substituted nucleobases [3] (namely uracil, thymine, and 2-TU), which evidenced the femtosecond to picosecond timescales for relaxation of the singlet $^1n\pi^*$ and $^1n\pi^*$ states as well as for intersystem crossing to the triplet manifold. In 2-TU, intersystem crossing occurs from the S_1 ($^1n\pi^*$) with near unity yields due to inaccessibility of conical intersections between the singlet excited states and the ground

E-mail addresses: mario.barbatti@univ-amu.fr (M. Barbatti), ullrich@physast.uga.edu (S. Ullrich). URL: http://www.barbatti.org (M. Barbatti).

^{*} Corresponding authors.

state [3,12,24,25]. The triplet population efficiently deactivates back to the ground state because of the small height of the barrier to the T_1/S_0 crossing point and large spin–orbit coupling constant [3,26]. In the case of the natural bases, uracil and thymine, intersystem crossing to the triplet manifold must compete with efficient internal conversion pathways from S_2 $(^1\pi\pi^*)$ and S_1 $(^1n\pi^*)$ back to the ground state [3,6,27]. Consequently, only a small fraction of the initially photoexcited S_2 $(^1\pi\pi^*)$ leads into the triplet manifold supported by temporary (picosecond) trapping in the S_1 $(^1n\pi^*)$ minimum. Intersystem crossing back to the ground state is unfavorable thanks to small spin–orbit coupling, and the population remains trapped for nanoseconds [3].

The intersystem crossing dynamics are affected by the excitation wavelengths, and a follow-up TR-PES study on 2-TU has shown a systematic decrease of time constants with increasing pump photon energy [10]. For example, time constants of 775 fs for population and 203 ps for depopulation of the triplet manifold are measured at 292 nm (4.25 eV), while at 249 nm (4.98 eV) they are only 207 fs and 48 ps, respectively. Under isolated, gas-phase conditions this is plausible since all excess energy remains inside the molecule during non-radiative relaxation processes. Energy barriers to access the $^1 n \pi^* / ^3 \pi \pi^*$ and the $^3 \pi \pi^* / ^3 \pi^*$ intersection seams control the intersystem crossing lifetimes to and from the triplet state, which is aided by the additional vibrational energy. In solution, the wavelengths dependence of the 2-TU photophysics is more complicated because the excess energy also dissipates into the surrounding environment [10].

To the best of our knowledge, no previous gas-phase time-resolved photoionization experiments of 4-TU have been reported, although vertical excitation energies and ionization energies are known from quantum chemical calculations, and the static photoelectron spectrum for the ground state ionization has been simulated [28-31]. Transient absorption spectroscopy experiments of related 4-thionated uracil and thymine derivatives in solution have shown complex photodynamics and strong solvent dependence of intersystem crossing lifetimes [9.14.32-34]. Most relevant to the present study, 335 nm photoexcitation of 4-TU in aqueous solution revealed ultrafast (within 240 fs) intersystem crossing to a long-lived triplet state [13]. Furthermore, time-resolved infrared studies on 4-TU in solution confirmed the formation of a long-lived triplet state with high quantum yield (0.9) upon UV irradiation [35]. Theoretical calculations indicate that vertical excitation energies of the S_1 ($^1n\pi^*$) may shift up to 0.4 eV due to solvent effects [31]. Given the critical role of the S_1 ($^1n\pi^*$) state in accessing the triplet manifold, the photodynamics observed in solution are not necessarily transferable to the gas-phase, which motivated the present study.

Here, TR-PES, supplemented by quantum-chemical calculations, is used to characterize internal conversion and intersystem crossing processes of excited 4-TU under gas-phase conditions. The excitation wavelength is varied across the UV absorption spectrum to investigate the effect of excess energy on the accessibility of conical intersections and crossing points. The results are compared to previous TR-PES measurements on the structural isomer 2-TU.

2. Experimental details

A detailed description of the apparatus used for the TR-PES experiments can be found in Refs. [2,36,37,38,39]. Briefly, the setup is based on a femtosecond laser system with UV conversion capabilities and a magnetic bottle photoelectron spectrometer. The laser system (Coherent Inc.) consists of a Ti:Sa oscillator (MIRA Optima 900) and a regenerative amplifier (Legend Elite), which pumps a traveling wave optical parametric amplifier (TOPAS-C) to produce tunable UV pulses. Wavelengths are set to 309.02, 330.15 and 347.2 nm (4.01, 3.76 and 3.57 eV) for photoexcitation with typical pulse energies of $4\,\mu\mathrm{J}$. The second harmonic of the amplifier fundamental provides $15{-}30\,\mu\mathrm{J}$ of $401.5\,\mathrm{nm}$ (3.09 eV), which serves as a two-photon photoionization probe. Both pump and time-delayed probe pulses are focused into the

ionization region of the photoelectron spectrometer by individual $50\,\mathrm{cm}$ focal length lenses and spatially overlapped at a small angle in the intersection region with a continuous molecular beam. The 4-TU powder is evaporated from a heated quartz sample holder at $160\,^{\circ}\mathrm{C}$, placed inside the nozzle and carried by a Helium backing gas. The most stable keto-thione tautomeric form of 4-TU [48,49] is expected to dominate the molecular beam. According to ab initio calculations, other tautomers are energetically disfavored by approximately $9\,\mathrm{kcal/mol}$ and were also absent in solution-phase infrared spectroscopic studies [47].

Time zero, i.e., the time of zero pump-probe delay, the Gaussian instrument response function (IRF), and energy calibrations are determined using a 50:50 gas mixture of 1.3-butadiene and helium. The dynamics and photoelectron spectra of 1,3-butadiene have previously been characterized for example by Ref. [58]. For the different excitation wavelengths the IRF is determined through TR-PES measurements and the full width at half maximum (FWHM) of the cross-correlation function is typically between 180 and 320 fs inside the ionization region of the magnetic bottle. Several factors contribute to the variation in FWHM, including laser beam characteristics (spatial and temporal) at the different wavelengths and the angle at which the pump and probe beams are overlapped. The magnetic bottle spectrometer is based on the principle of a time-of-flight measurement for photoelectrons to travel from the ionization region to the detector. Peaks of known energy in the butadiene photoelectron spectrum are used for time-of-flight to energy conversion. To obtain accurate calibration constants positive and negative acceleration voltages are applied in the ionization region to shift butadiene peaks across the relevant time-of-flight range.

3. Computational details

The geometries of the ground and excited states of 4-TU were respectively optimized with the Møller–Plesset perturbation theory to the second order (MP2) and the algebraic diagrammatic construction to second order (ADC(2)) levels in the gas phase [40,41]. The Dunning's aug-cc-pVDZ basis set was used for all calculations [42]. Calculations were done with frozen core and applying the resolution-of-identity (RI) approximation for the computation of two-electron integrals. The singlet/singlet and singlet/triplet intersection minima between different states were optimized with an in-house modified version of the CIOpt program [43]. Reaction paths were computed applying linear interpolation in natural internal coordinates (LIIC) [44]. ADC(2) and MP2 calculations were done with Turbomole [45]. Additional information about the calculations, including Cartesian coordinates of all minima and crossings are provided in the Supplementary Information (SI).

4. Discussion

Fig. 1 presents the UV absorption spectrum of 4-TU [13], and the underlying transitions obtained from the ADC(2) calculation are overlaid as a stick spectrum colored in red. The experimental spectrum shows the first absorption band with maximum at 330 nm (3.76 eV) followed by a second, weaker band centered around 240 nm (5.17 eV). Vertical excitation energies of 2.86, 4.01, and 4.82 eV and oscillator strengths of 0.000, 0.399, and 0.006 have been calculated for the lowest singlet excited states S_1 ($^1n\pi^*$), S_2 ($^1\pi\pi^*$), and S_3 ($^1\pi\pi^*$), respectively. Compared to the band maximum of the experimental spectrum, the ADC(2) vertical excitation energy of the S_2 ($^1\pi\pi^*$) state is blue-shifted by 0.25 eV. This shift is not necessarily caused by accuracy issues, as the vertical excitation and the band maximum are usually displaced by 0.1-0.2 eV [46]. For sake of comparison, the ADC(2) vertical excitations are also shown displaced by 0.25 eV as a grey dashed stick spectrum, showing a perfect match with the experimental bands. It should be noted that the UV spectrum presented in Fig. 1 was recorded in aqueous solution and primarily serves for illustration [13]. Based on

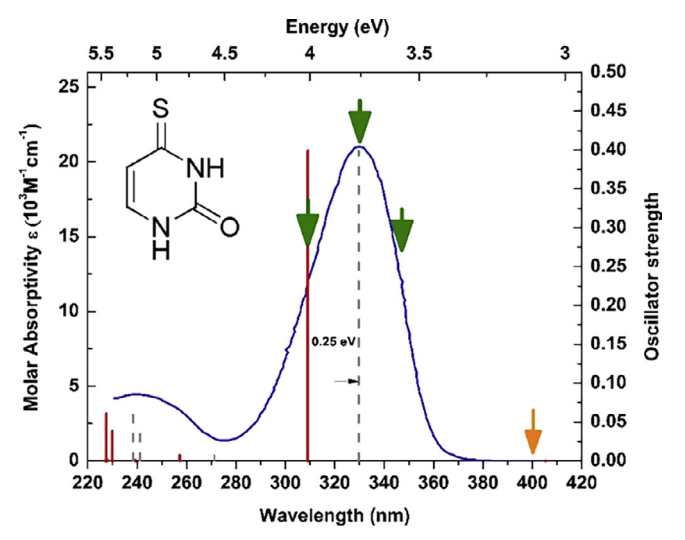


Fig. 1. Molar absorptivity of the 4-TU in aqueous phosphate-buffered saline solution, PH 7.4 from Ref. [13]. The green arrows are pump wavelengths at 309.02, 330.16 and 347.2 nm and the orange arrow locates the probe wavelength at 401.5 nm. The solid red lines are the calculated excited state transition energies with lengths indicating their oscillator strengths. The dashed grey lines are shifted by 0.25 eV to align with the experimental spectrum. The X-axis shows a wavelength scale at the bottom and equivalent photon energies at the top. The Y-axis at left is the molar absorptivity ϵ ($10^3 \, \text{M}^{-1} \text{cm}^{-1}$) for the experimental absorption spectrum, whereas the Y-axis at the right shows the oscillator strength of the calculated transitions. The most stable keto-thione tautomeric form of the 4-TU [47–49] is presented in the left-top corner of the figure. (For interpretation of the references to color in this figure legend, the reader is referred to the web version of this article.)

calculations by Ref. [31], close similarities between the gas and condensed phase absorption spectra can be expected for the region of interest. Calculated solvent effects on the S_2 ($^1\pi\pi^*$) transition energy are minimal (< 0.05 eV) and the S_1 ($^1n\pi^*$), which blue-shifts by ~0.4 eV upon solvation, does not contribute to the absorption spectrum due to its insignificant oscillator strength.

The green arrows in Fig. 1 indicate the pump wavelengths at 309.02, 330.16, and 347.2 nm, and are associated with excitation to the S_2 state of ${}^1\pi\pi^*$ character. The orange arrow shows the probe wavelength at 401.5 nm, just below the onset of the UV absorption spectrum to minimize contributions from unwanted probe-pump signals. A twophoton process is required for photoionization of the electronically excited states given a vertical ground-state ionization energy of approximately 8.75 eV [29]. According to the computed S₀-photoelectron spectrum in Ref. [29], the lowest energy band (IP1) falls within the 8–10 eV region with contributions from sulfur localized n- (D_0) and π holes (D₁). The second photoelectron band with ionizations of oxygenlocalized orbitals is energetically inaccessible with the total photon energies employed in our TR-PES studies [29]. The analysis of our TR-PES spectra relies on ionization correlations between the electronically excited and ionic states. In analogy with our previous study on 2-TU [10], it is expected that the planar $S_2(^1\pi\pi^*)$, $S_1(^1n\pi^*)$, and triplet state minima — which all originate from sulfur localized orbital excitations — preferentially ionize into IP1, and the calculation has confirmed this prediction. At the highest pump photon energy, the twisted S_2 ($^1\pi\pi^*$), with oxygen-localized excitations, can be reached, but probe photon energies employed in the present study are insufficient to access IP2 with oxygen localized n- (D_2) and π -holes (D_3) .

Fig. 2 shows the 4-TU TR-PES results with excitation wavelengths decreasing from top to bottom. The first column displays the TR-PES spectrum from the experiment abbreviated to $\sim\!5$ ps for clarity. The 2D spectrum is plotted as a function of pump–probe delay versus electron binding energy, which is calculated by subtracting the measured photoelectron kinetic energy from the total photon energy of the $1+2^{\prime}$

multiphoton excitation-ionization process. The cutoff of the TR-PES spectrum at high electron binding energies hence corresponds to the total photon energy. The 2D TR-PES spectra are best described by a model based on sequential dynamics consisting of three exponential decays (with Gaussian convolution). The use of fewer decays in the fitting function leads to systematic residuals. Global analysis of the 2D TR-PES spectra yields the decay associated spectra (DAS, second column), which are plotted with signal intensities normalized to the amplitude of their time traces and identical energy axes. The rapid drop in the photoelectron signal at high electron binding energies is attributed to a decrease in collection efficiency for low kinetic energy electrons, rather than to the inherent shape of the molecular photoelectron band. The time traces (third column) describing the dynamics are displayed for the entire pump-probe delay range, with contributions plotted in a matching color scheme as the DAS. The time constants extracted from these fits are summarized in Table 1. Additional 2D fit results including residuals are provided in the SI.

Upon visual inspection, all 4-TU TR-PES spectra generally display similar 2D spectra, DAS, and dynamics with systematic trends as the excitation wavelength is changed. Upon increasing vibrational excitation, photoelectron spectra shift towards higher electron binding energies, and time constants decrease because conical intersections become more easily accessible. The fitting equation underlying the data analysis implies that the deactivation pathway involves a three-step process and is, therefore, suggested to be the same, general mechanism also observed in 2-TU [10] and other thiobases [9]: ultrafast internal conversion from the S_2 ($^1\pi\pi^*$) to the S_1 ($^1n\pi^*$) state, which then acts as the doorway to populate the long-lived triplet manifold. To corroborate this photophysical model and also investigate the differences between the photodynamics of 4-TU and 2-TU, a thorough analysis of the TR-PES data based on supportive ab initio calculations follows. Table 2 collects the excitation and ionization energies for characteristic geometries of relevant ground and electronically excited states.

Employing a pump wavelength of 347.2 nm, see Fig. 2, row 1. photoexcitation proceeds to the bright S_2 ($^1\pi\pi^*$) state with excess energy of approximately 0.42 eV above the planar (P) S2 minimum. Photoionization produces a photoelectron band (column 2, blue line) with an onset around 8.2 eV with increasing signal from approximately 8.6 to 9.25 eV, and likely beyond the low electron kinetic energy dropoff (~9.5 eV). The band is shifted slightly toward higher electron binding energies compared to the vertical ionization potential calculated for the planar S_2 minimum ($D_1 = 9.02 \,\text{eV}$), a feature that is common to these types of rigid, heterocyclic molecules [2,10,50,51]. During the relaxation from the Franck-Condon region to the planar S₂ minimum, excess energy is converted into vibrational excitation. In a simple picture, assuming a $\Delta \nu = 0$ propensity rule, the vibrational excitation is transferred to the cationic state upon photoionization. Here, ionization into the cationic state, D_1 , which corresponds to a π hole, is expected with up to 0.42 eV vibrational excitation, in line with the experimentally observed shift of the photoelectron band in the electron binding energy plot in column 2. A second S2 minimum featuring a twisted (T) ring exists, but its energy is too high to be populated at

This first photoelectron band decays within ~ 200 fs (column 3, blue line) as another band in the electron binding energy range from 8.8 eV to the ~ 9.5 eV drop-off rises, indicating ultrafast internal conversion to a lower-lying singlet excited state (S₁). Given that the total energy (electronic and vibrational excitation) of the molecules amounts to 3.57 eV (the pump photon energy), only the S₂/S₁ crossing seam in the planar (P) region, which connects the planar S₂ minimum to S₁, is accessible. Note that in Table 2 the energy of this intersection is 3.75 eV, 0.2 eV above the total energy. This inconsistency may be mainly attributed to low accuracy of the optimization procedure based on the penalty function approach [52]. At the S₁ minimum, the total vibrational excitation gained due to internal conversions since the Franck Condon region already amounts to 1.08 eV. Although the ab initio

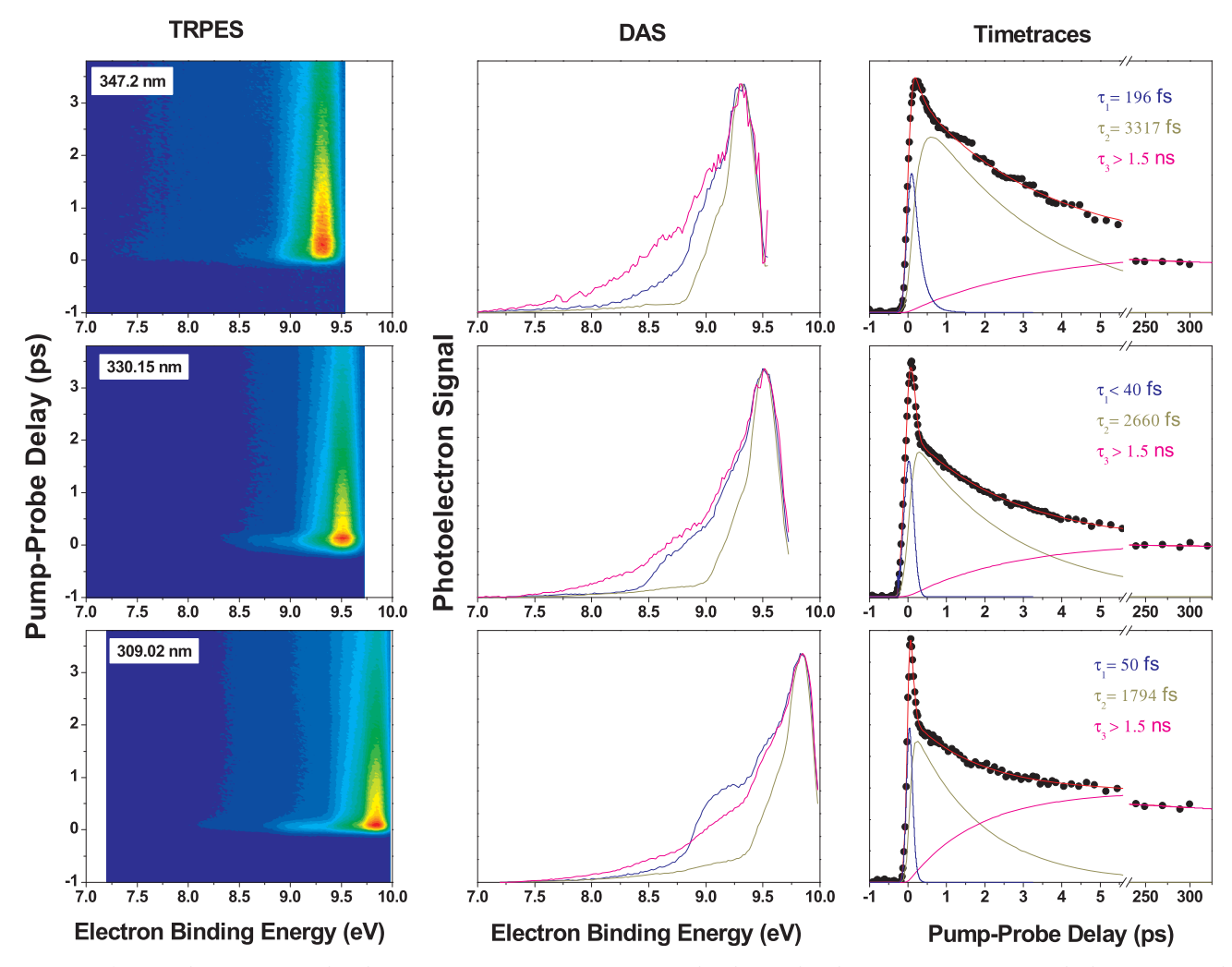


Fig. 2. TR-PES of 4-TU with excitation wavelengths at 309.02 nm, 330.16 nm, 347.2 nm and probe wavelength at 401.5 nm in a 1 + 2′ multiphoton process. Global analysis of the TRPES spectra (column 1) yields the decay associated spectra (column 2) and timetraces (column 3), the latter plotted for the entire pump–probe delay range. (Blue: short-lived decay less than 200 fs; dark yellow, intermediate decay of a few ps; magenta, long-lived decay of nanosecond timescale). Signal (dots), Fit (red solid line). (For interpretation of the references to color in this figure legend, the reader is referred to the web version of this article.)

Table 1Time constants for the three-step relaxation process in 4-TU. The time constants were extracted by fitting a Gaussian convoluted sequential decay consisting of three exponentials to the long-range TR-PES data set.

	Pump wavelength (nm)	Pump energy (eV)	τ_1 (fs)	τ_2 (fs)	τ_3 (ns)	
•	309.02	4.01	50 ± 10	1794 ± 150	> 1.5	
	330.16	3.76	< 40	2660 ± 250	> 1.5	
	347.20	3.57	196 ± 40	3317 ± 300	> 1.5	

ionization energy for the S_1 minimum geometry to the lowest n-hole is calculated to be $D_0=8.61\,\mathrm{eV}$, such excess of vibrational energy should shift the photoelectron band by up to $1.08\,\mathrm{eV}$, to even higher electron binding energies. This shift is best visible for the onset of the blue and dark yellow DAS spectra (column 2). It should be emphasized here that, with a total amount of $1.08\,\mathrm{eV}$ vibrational excitation, parts of the photoelectron band shift outside the energy window observable with our total photon energy, which prevents further analysis based on a comparison of band maxima. Nevertheless, even the partial observation of the DAS allows for accurate extraction of the decay dynamics of the S_1 state, whose lifetime was measured to be approximately $3.3\,\mathrm{ps}$.

Subsequently, a long-lived ($> 1.5\,\mathrm{ns}$) state is populated with a negligible shift in the DAS. This is consistent with an assignment to the triplet states, T_2 and T_1 , which have minimum energies and ionization

potentials similar to the S_1 state, as shown in Table 2. Noteworthy is a relative increase in photoelectron signal extending towards lower electron binding energies. Tentatively this is associated with vibrational energy redistribution and equilibration over extended timescales, which reshapes the envelope of the photoelectron band.

To provide an easy visual comparison, the theoretical results are graphed in Fig. 3. Assuming the $\Delta \nu = 0$ propensity rule, the electron binding energy *BE* for a geometry **R** is estimated as (see SI)

$$BE(R) \approx E_{pump} + E_{D_m}(R) - E_{S_i}(R)$$
 (1)

where E_x is the potential energy of state X computed at \mathbf{R} , D_m is the target cation state, and S_i is the neutral state before ionization. Using Eq. (1) and the data from Table 2, the binding energies for the main geometries visited during the photodynamics are calculated and shown in Fig. 3, bottom, arranged as a function of the experimental times. Comparing this figure and the TR-PES in Fig. 2 (row 1, column 1), the proposed pathway qualitatively describes the main features of the measured spectrum. Note in particular the strong shift to large BE between the Franck-Condon region ($V_{\rm exc}$) and the S_1 minimum. After that, the BE tends to be approximately constant until the S_0 is populated and a new strong shift is predicted. Based on this analysis, the relaxation is proposed to proceed along a pathway that directly connects the planar S_2 ($^1\pi\pi^*$) minimum via a conical intersection with the S_1 ($^1n\pi^*$) minimum, from where it advances to the close-lying triplet manifold

Table 2 Summary of singlet, triplet, and doublet (cation) results for characteristic minima (min), conical intersections (CI), and intersystem crossing (ISC) geometries of 4-TU computed at the ADC(2) level. CI and ISC were optimized until an energy gap equal or smaller than $0.02 \, \text{eV}$ was reached. All energies (eV) relative to the S_0 state minimum. The main diabatic character is indicated for each case in parenthesis. The oscillator strength for the vertical excitations from the S_0 minimum is given in square brackets. When relevant, planar (P) and ring twisted (T) geometries are labeled.

Geometry	Energies (eV)								
	S ₀ (¹ cs)	$S_1 (^1 n \pi^*)$	$S_2(^1\pi\pi^*)$	$T_1 (^3n\pi^*)$	$T_2 (^3\pi\pi^*)$	D_0	D_1		
S ₀ min	0.00	2.86 [0.000]	4.01 [0.399]	2.71	2.76	8.54 (² n)	8.91 (² π)		
S ₁ min	0.43	2.49	3.35	2.41	2.47	8.61 (² n)	$8.88 (^2\pi)$		
S ₂ min (P)	1.00	2.66	3.15	2.63	2.67	8.87 (² n)	$9.02~(^2\pi)$		
S ₂ min (T)	1.32	3.45	4.15^{a}	3.32	3.42	10.10 (² n)	$10.50~(^2\pi)$		
T ₁ min	0.36	2.49	3.41	2.41	2.47	8.59 (² n)	$8.88 (^2\pi)$		
T ₂ min	0.34	2.53	3.41	2.44	2.44	8.60 (² n)	$8.85 (^2\pi)$		
S ₂ /S ₁ CI (P)		3.73	3.75			$9.99~(^2\pi)$	10.02 (² n)		
S ₂ /S ₁ CI (T)		4.40	4.40			$11.62~(^2\pi)$	11.62 (² n)		
S ₁ /T ₂ ISC		2.49			2.47	8.60 (² n)	$8.87~(^2\pi)$		
T ₁ /S ₀ ISC	3.11			3.13		10.69 (² n)	$11.35~(^2\pi)$		

 $^{^{}a}(^{1}n\pi^{*} + ^{1}\pi\pi^{*})$ at the C=O.

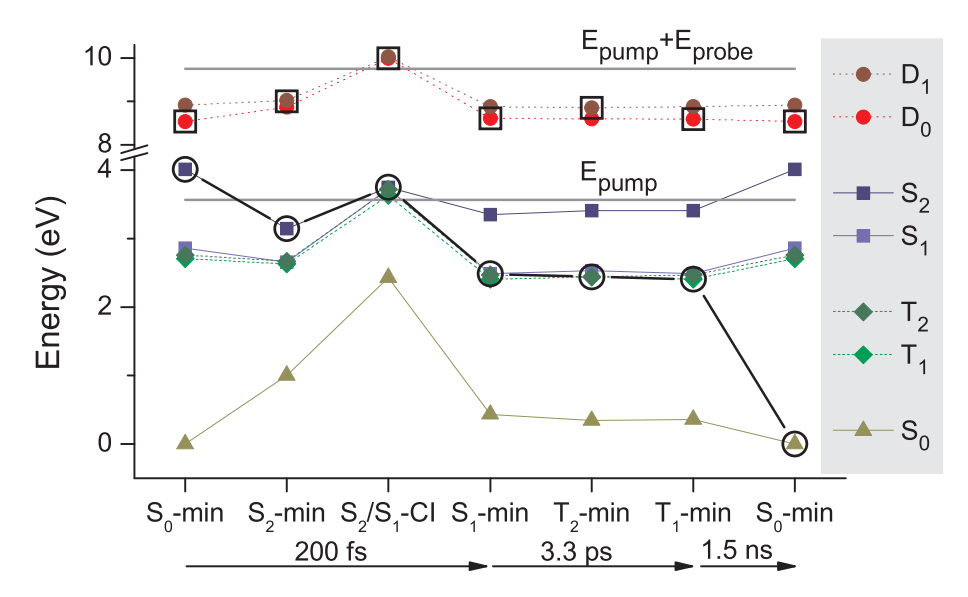
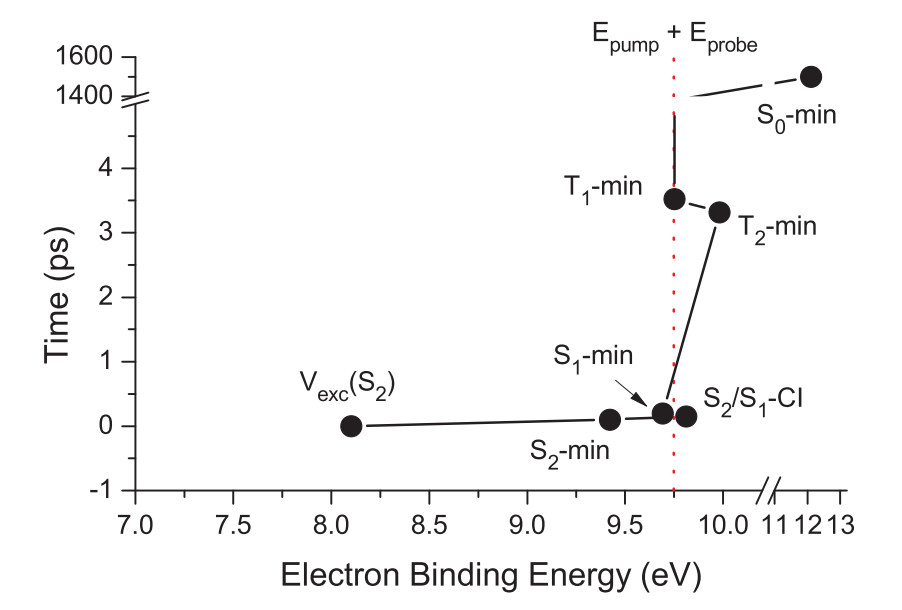


Fig. 3. Top: Electronic energy of the main minima and intersections visited during the photodynamics of 4-TU according to ADC(2) results. The current state populated at each step is indicated by the open circle. The respective target cation state is indicated by the open square. Bottom: Theoretical estimate of the electron binding energy for the main minima and intersections visited during dynamics. They are arranged as a function of time to be directly compared to the TR-PES in Fig. 2, row 1, column 1. In both figures, the indicated pump energy corresponds to the 347.2-nm setup. Also in both figures, the time lags are those from the experimental fitting.



and is trapped, until it moves back to S_0 much later (Fig. 3, top).

To investigate the effects of the vibrational energy excess on the photophysical pathway and dynamics, the discussion proceeds with the 330.16 and 309.02 nm TR-PES data (Fig. 2, row 2 and 3), which are analyzed similarly. The DAS associated with the ultrafast decay dynamics τ_1 (blue line) maintains its general shape consisting of three broad features, but the rising edge of the photoelectron band shifts from 8.2 eV (at 347.2 nm) to 8.4 eV (at 330.16 nm) to 8.7 eV (309.02 nm), corresponding roughly to the increase in pump photon energy and hence the additional vibrational excitation of the molecule. Similarly, comparing the rising edge of the DAS associated with the ps contribution (τ_2) , a 0.2–0.3 eV shift is observed at each time when the wavelength is changed, and as discussed above, the long-lived (τ_3) DAS follows accordingly. The estimated BEs for these pump wavelengths, analogous to Fig. 3-bottom, are provided in the SI.

Unless there are changes in the general pathway, time constants can be expected to decrease as a function of higher pump photon energy due to easier accessibility of crossing points and conical intersections in the vibrationally excited molecule. The behavior of τ_1 shows a different trend, although one needs to be cautious not to overinterpret the time constants that fall within the cross-correlation of the experiment. For 347.2 nm excitation, τ_1 is measured to be around 196 fs, which is significantly longer than the time constants at the other wavelengths. This is not surprising given that the total energy deposited into the molecule by the pump photon equals 3.571 eV, similar to the calculated energy of the conical intersection $(S_2/S_1 \text{ CI (P)})$ between the planar S_2 and S_1 states. Hence, all available excess energy must flow into the coordinate leading to the conical intersection for internal conversion. This conical intersection is more easily reached at higher pump photon energies, resulting in a shorter S_2 lifetime of $< 40\,\mathrm{fs}$ for 330.16 nm excitation. [57] Intriguing, however, is the increase of τ_1 to 50 fs at 309.16 nm, when even more energy is available for the internal conversion process and may be indicative of a change in the relaxation pathway. One may speculate that the increased lifetime is due to the involvement of the twisted S₂ (T) minimum, which becomes accessible following 309.16 nm photoexcitation. The present experiments, however, are mostly blind to dynamics involving the S_2 (T) minimum, which features a high vertical ionization potential of $\sim 10 \, \text{eV}$ and is outside the range of our probe photon energy. Nevertheless, some ionization into the lower ionization potentials may be expected, which would contribute to the photoelectron signals at lower electron binding energies. A fraction of the population may temporarily evolve into S2 (T) minimum, but, due to the inaccessibility of the twisted conical intersection S2/S1 CI (T), it returns to the planar pathway and hence increases the measured time constant τ_1 . Photoexcitation of a higher-lying singlet excited state S_3 may provide another potential explanation for the longer τ_1 , in analogy with the observations in 2-TU [10]. The additional S₃ to S₂ internal conversion step typically occurs on ultrafast timescales, similar to S₂ relaxation, and within the cross-correlation of the experiment. These processes are indistinguishable by data fitting and instead a slight increase in τ_1 would be observed. The present calculation, however, locates the S3 state in 4-TU above the reach of the employed pump

Time constant τ_2 displays the expected systematic trend, which suggests that the pathway for intersystem crossing from S_1 ($^1n\pi^*$) onto the triplet manifold ($^3\pi\pi^*$) is maintained at all excitation wavelengths, but the intersection is more easily accessed with additional vibrational excitation. The pump–probe range employed in our experiments does not capture the decay dynamics of the long-lived triplet states and only allows us to determine a lower limit ($\tau_3 > 1.5$ ns) for intersystem crossing back to the ground state.

In comparing the photodynamics of 2-TU and 4-TU, the effect of the sulfur substituent position is assessed. Intersystem crossing time constants are generally much slower in 4-TU than in 2-TU, with τ_2 of hundreds fs and τ_3 of tens to a few hundred ps for the latter, and a systematic decrease in time constants as the excess energy increases

[10]. For example, when comparing photoexcitation at the absorption maximum of each molecule (271 nm for 2-TU and 330.16 nm for 4-TU), population of the triplet manifold from S_1 ($^1n\pi^*$) occurs within 333 fs versus 2.66 ps for 2-TU and 4-TU, respectively. This difference reflects the remarkable distinction between the excited state topographies of the 2- and 4-thiosubstituted species, starting with the absorption spectrum: it is not only red shifted by about 0.8 eV in 4-TU, but while in this molecule it is formed by a single $^1\pi\pi^*$ excitation, in 2-TU it merges two distinct $^1\pi\pi^*$ bands [10,22]. Moreover, at the $^1n\pi^*$ planar S_1 minimum, the 2-thiosubstituted species has larger spin–orbit coupling to the triple manifold than the 4-thiosubstituted species [53].

The most striking difference between 2-TU and 4-TU photodynamics is observed in the third time constant τ_3 . While pumping 2-TU at the band maximum (271 nm) leads to $\tau_3 = 109 \, \text{ps}$ [10], the present work shows that excitation of 4-TU at its band maximum (330.16 nm) results in $\tau_3 > 1.5$ ns. The reason underlying these strongly distinct behaviors is the triplet state topography of the two molecules: while the T₁ state of 2-TU shows a ${}^3\pi\pi^*$ double-well [10], the T₁ state of 4-TU features a ${}^3n\pi^*$ minimum. Depopulation of the lowest triplet state of 2-TU requires surmounting a 0.2 eV barrier to access the intersection to S₀ [10]. In 4-TU in contrast, this intersection is located 0.72 eV above the T₁ minimum (Table 2), leading to the extended trapping beyond the observation window of the present experiments. Another factor contributing to the elongated triplet decay of 4-TU is the spin-orbit coupling. As shown for thiothymine in Ref. [53], the total coupling of the triplet states (T1 and T2) with S0 is about twice as large for sulfur in position 2 than in position 4.

5. Conclusions

The present study highlights the importance of a "planar pathway" in the relaxation dynamics of photoexcited 4-TU as opposed to the previously proposed "twisted pathway" [9,14,44]. The latter directly connects the second, higher S_2 (T) minimum via a conical intersection, both involving twisted molecular geometries, to the lower-lying S_1 ($^1n\pi^*$) state.

To characterize the relaxation along the planar pathway selectively, TR-PES experiments were performed at three different excitation wavelengths, which photoexcited 4-TU to the vibrationally excited planar $S_2 \left(^1\pi\pi^* \right)$ but with insufficient energy to access the twisted conical intersection. Experimental observations are in excellent agreement with computed potential energy profiles, minima, crossing points, and estimates of electron binding energy.

Fig. 4 summarizes the ab initio energy profiles connecting planar and twisted geometries. The planar pathway observed in the present TR-PES study is indicated by a sequence of solid arrows. Vertical photoexcitation to a vibrationally excited S_2 ($^1\pi\pi^*$) state is represented by horizontal lines for pump wavelengths of 347.2, 330.16, and 309.02 nm. After fast relaxation to the planar S_2 minimum (a) followed by internal conversion at the planar S_2/S_1 intersection, the S_1 ($^1n\pi^*$) state is populated within less than 200 fs (b). A lifetime of a few picoseconds is measured for the S_1 ($^1n\pi^*$), which undergoes intersystem crossing to the triplet manifold (c). The triplet state decays at times longer than 1.5 ns (d).

The photodynamics leading from the S_2 ($^1\pi\pi^*$) state up to the population of the lowest triplet excited state qualitatively resembles those of 2-TU, although the time constants are remarkably distinct. This difference is especially pronounced in the intersystem crossing back to the ground state, which is strongly dependent on the position of the substituent. In stark contrast to 2-TU, which efficiently intersystem crosses back to the ground state, the population remains trapped on the lowest triplet excited state of 4-TU. This is consistent with the theoretical prediction of a higher activation barrier in the case of 4-TU and further supported by the observation of phosphorescence [34,54–56] in other 4-TU derivatives.

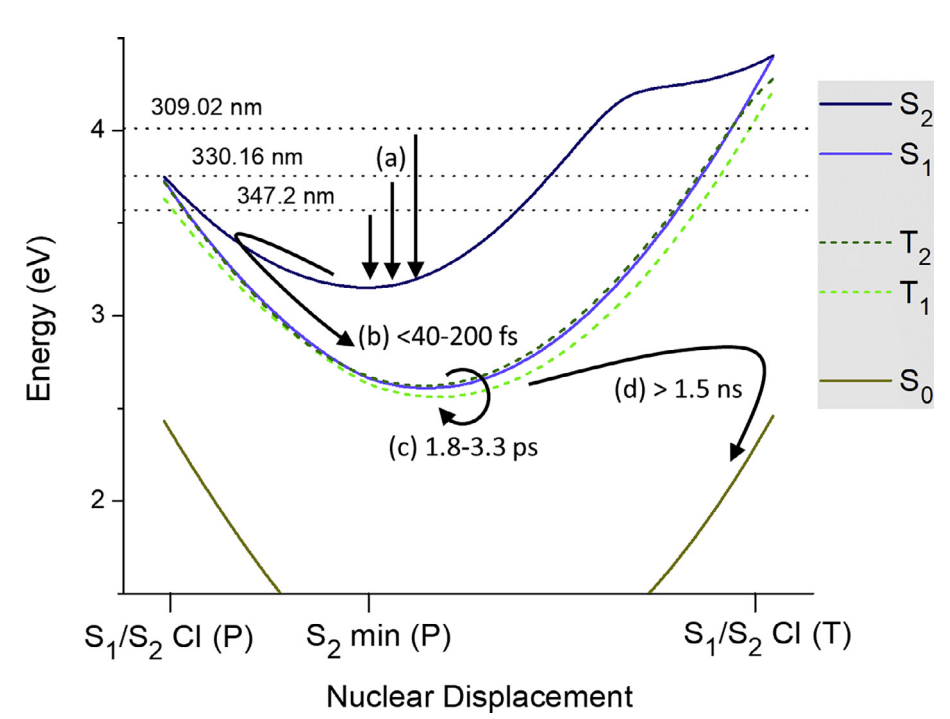


Fig. 4. Energy profiles connecting the planar (P) S_2 minimum to the planar S_2/S_1 conical intersection (left) and the twisted S_2/S_1 conical intersection (T, right). The horizontal lines indicate the pump energies employed in the experiments. The arrows indicate the relaxation pathway proposed in this study together with the time lags from the TR-PES fitting.

Acknowledgments

This work was supported by the National Science Foundation Grant NSF-CHE-1362237 and 1800050. MB and SB thank the support of the Excellence Initiative of Aix-Marseille University (A*MIDEX) and the project Equip@Meso (ANR-10-EQPX-29-01), both funded by the French Government "Investissements d'Avenir" program. MB also acknowledges funding from the WSPLIT project (ANR-17-CE05-0005-01).

Appendix A. Supplementary data

Supplementary data associated with this article can be found, in the online version, at https://doi.org/10.1016/j.chemphys.2018.08.011.

References

- [1] A.A. Beckstead, Y. Zhang, M.S. de Vries, B. Kohler, Phys. Chem. Chem. Phys. 18 (2016) 24228.
- [2] N.L. Evans, S. Ullrich, J. Phys. Chem. A 114 (2010) 11225.
- [3] H. Yu, J.A. Sanchez-Rodriguez, M. Pollum, C.E. Crespo-Hernández, S. Mai, P. Marquetand, L. González, S. Ullrich, Phys. Chem. Chem. Phys. 18 (2016) 20168.
- [4] K. Kleinermanns, D. Nachtigallová, M.S. de Vries, Int. Rev. Phys. Chem. 32 (2013) 308.
- [5] M. Barbatti, A. Borin, S. Ullrich, Photoinduced Phenomena in Nucleic Acids I, Springer International Publishing, 2015, p. 1.
- [6] H.R. Hudock, B.G. Levine, A.L. Thompson, H. Satzger, D. Townsend, N. Gador, S. Ullrich, A. Stolow, T.J. Martinez, J. Phys. Chem. A 111 (2007) 8500.
- [7] T. Gustavsson, R. Improta, D. Markovitsi, J. Phys. Chem. Lett. 1 (2010) 2025.
- [8] B. Kohler, J. Phys. Chem. Lett. 1 (2010) 2047.
- [9] S. Arslancan, L. Martínez-Fernández, I. Corral, Molecules 22 (2017) 998.
- [10] J.A. Sanchez-Rodriguez, A. Mohamadzade, S. Mai, B. Ashwood, M. Pollum, P. Marquetand, L. Gonzalez, C.E. Crespo-Hernandez, S. Ullrich, Phys. Chem. Chem. Phys. 19 (2017) 19756.
- [11] S. Mai, M. Pollum, L. Martínez-Fernández, N. Dunn, P. Marquetand, I. Corral, C.E. Crespo-Hernández, L. González, Nat. Commun. 7 (2016) 13077.
- [12] J.P. Gobbo, A.C. Borin, Comput. Theor. Chem. 1040–1041 (2014) 195.
- [13] M. Pollum, S. Jockusch, C.E. Crespo-Hernández, Phys. Chem. Chem. Phys. 17 (2015) 27851.
- [14] L. Martínez-Fernández, G. Granucci, M. Pollum, C.E. Crespo-Hernández, M. Persico, I. Corral, Chem.-Eur. J. 23 (2017) 2619.
- [15] S. Prachayasittikul, A. Worachartcheewan, C. Nantasenamat, M. Chinworrungsee, N. Sornsongkhram, S. Ruchirawat, V. Prachayasittikul, Eur. J. Med. Chem. 46 (2011) 738.
- [16] L. Dencker, B. Larsson, K. Olander, S. Ullberg, Br. J. Cancer 45 (1982) 95.
- [17] G. Trigiante, Y.-Z. Xu, Photodynamic Therapy: Fundamentals, Applications and Health Outcomes, Nova Science Publishers, Inc., 2015.
- [18] M. Pollum, L. Guan, S. Ahsanuddin, E. Baron, M. Lam, C. Crespo-Hernandez, J.

Invest. Dermatol. 136 (2016) S105.

- [19] M. Pollum, L. Martínez-Fernández, C.E. Crespo-Hernández, Photoinduced Phenomena in Nucleic Acids I, Springer, Cham, 2015, p. 245.
- [20] S. Matsika, Photoinduced Phenomena in Nucleic Acids I, Springer, Cham, 2015, p. 209.
- [21] C.E. Crespo-Hernández, Molecules 22 (2017) 2203.
- [22] S. Bai, M. Barbatti, J. Phys. Chem. A 120 (2016) 6342.
- [23] M. Pollum, C.E. Crespo-Hernández, J. Chem. Phys. 140 (2014) 071101.
- [24] S. Mai, P. Marquetand, L. González, J. Phys. Chem. Lett. 7 (2016) 1978.
- [25] S. Mai, P. Marquetand, L. González, J. Phys. Chem. A 119 (2015) 9524.
- [26] S. Bai, M. Barbatti, Phys. Chem. Chem. Phys. 19 (2017) 12674.
- [27] L. Stojanović, S. Bai, J. Nagesh, A. Izmaylov, R. Crespo-Otero, H. Lischka, M. Barbatti, Molecules 21 (2016) 1603.
- [28] M. Shukla, J. Leszczynski, J. Phys. Chem. A 108 (2004) 7241.
- [29] M. Ruckenbauer, S. Mai, P. Marquetand, L. González, J. Chem. Phys. 144 (2016) 074303.
- [30] M. Shukla, J. Leszczynski, J. Mol. Struct. Theochem. 771 (2006) 149.
- [31] M. Shukla, J. Leszczynski, J. Phys. Chem. A 108 (2004) 10367.
- [32] Y. Harada, C. Okabe, T. Kobayashi, T. Suzuki, T. Ichimura, N. Nishi, Y.-Z. Xu, J. Phys. Chem. Lett. 1 (2009) 480.
- [33] C. Reichardt, C.E. Crespo-Hernández, Chem. Commun. 46 (2010) 5963.
- [34] C. Reichardt, C.E. Crespo-Hernández, J. Phys. Chem. Lett. 1 (2010) 2239.
- [35] X. Zou, X. Dai, K. Liu, H. Zhao, D. Song, H. Su, J. Phys. Chem. B 118 (2014) 5864.
- [36] H. Yu, N.L. Evans, A.S. Chatterley, G.M. Roberts, V.G. Stavros, S. Ullrich, J. Phys. Chem. A 118 (2014) 9438.
- [37] H. Yu, N.L. Evans, V.G. Stavros, S. Ullrich, Phys. Chem. Chem. Phys. 14 (2012) 6266.
- [38] N.L. Evans, H. Yu, G.M. Roberts, V.G. Stavros, S. Ullrich, Phys. Chem. Chem. Phys. 14 (2012) 10401.
- [39] T. Godfrey, H. Yu, S. Ullrich, J. Chem. Phys. 141 (2014) 044314.
- [40] A.B. Trofimov, J. Schirmer, J. Phys. B: At., Mol. Opt. Phys. 28 (1995) 2299.
- [41] J. Schirmer, Phys. Rev. A 26 (1982) 2395.
- [42] T.H. Dunning Jr., J. Chem. Phys. 90 (1989) 1007.
- [43] B.G. Levine, J.D. Coe, T.J. Martínez, J. Phys. Chem. B 112 (2008) 405.
- 44] G. Fogarasi, X. Zhou, P.W. Taylor, P. Pulay, J. Am. Chem. Soc. 114 (1992) 8191.
- [45] R. Ahlrichs, M. Bär, M. Häser, H. Horn, C. Kölmel, Chem. Phys. Lett. 162 (1989) 165.
- [46] F.J. Avila Ferrer, J. Cerezo, E. Stendardo, R. Improta, F. Santoro, J. Chem. Theory Comput. 9 (2013) 2072.
- [47] A. Psoda, Z. Kazimierczuk, D. Shugar, J. Am. Chem. Soc. 96 (1974) 6832.
- [48] Y.V. Rubin, Y. Morozov, D. Venkateswarlu, J. Leszczynski, J. Phys. Chem. A 102 (1998) 2194.
- [49] T. Marino, N. Russo, E. Sicilia, M. Toscano, Int. J. Quantum Chem. 82 (2001) 44.
- [50] T. Godfrey, H. Yu, M.S. Biddle, S. Ullrich, Phys. Chem. Chem. Phys. 17 (2015) 25197.
- [51] R. Crespo-Otero, M. Barbatti, H. Yu, N.L. Evans, S. Ullrich, ChemPhysChem 12 (2011) 3365.
- 52] T.W. Keal, A. Koslowski, W. Thiel, Theor. Chem. Acc. 118 (2007) 837.
- [53] X. Gao, S. Bai, D. Fazzi, T. Niehaus, M. Barbatti, W. Thiel, J. Chem. Theory Comput. 13 (2017) 515.
- [54] G. Wenska, K. Taras-Goślińska, A. Łukaszewicz, G. Burdziński, J. Koput, A. Maciejewski, Photochem. Photobiol. Sci. 10 (2011) 1294.

- [55] K. Taras-Goślińska, G. Wenska, B. Skalski, A. Maciejewski, G. Burdziński,
- J. Karolczak, J. Photochem. Photobiol. A 168 (2004) 227. [56] Y. Harada, T. Suzuki, T. Ichimura, Y.-Z. Xu, J. Phys. Chem. B 111 (2007) 5518. [57] A time constant of $\tau_1=20\pm15$ fs was obtained from the fit to the 330.16 nm TRPES data. In general, the extraction of time constants shorter than the cross-
- correlation is possible as long as parameters such as the pulse duration and time of pump-probe overlap are known. For example, see Stolow and co-worker, J. Phys. Chem. A, 106 (2002), 8979.
- [58] O. Schalk, A.E. Boguslavskiy, A. Stolow, J. Phys. Chem. Lett. 5 (2014) 560.